This article was downloaded by: [IIT Indian Institute of Technology - Mumbai]
On: 11 July 2012, At: 07:24
Publisher: Taylor & Francis
Informa Ltd Registered in England and Wales Registered Number: 1072954 Registered office: Mortimer House, 37-41 Mortimer Street, London W1T 3JH, UK

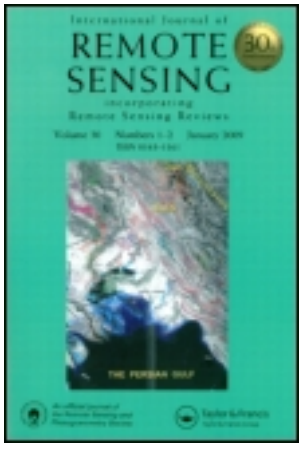

International Journal of Remote Sensing

Publication details, including instructions for authors and subscription information:
http://www.tandfonline.com/loi/tres20

Spectral pathways for effective delineation of high-grade bauxites: a case study from the Savitri River Basin, Maharashtra, India, using EO-1 Hyperion data

K. N. Kusuma [a], D. Ramakrishnan [a] & H. S. Pandalai [a]

[a] Department of Earth Sciences, Indian Institute of Technology, Mumbai, 400076, India

Version of record first published: 11 Jul 2012

To cite this article: K. N. Kusuma, D. Ramakrishnan & H. S. Pandalai (2012): Spectral pathways for effective delineation of high-grade bauxites: a case study from the Savitri River Basin, Maharashtra, India, using EO-1 Hyperion data, International Journal of Remote Sensing, 33:22, 7273-7290

To link to this article: http://dx.doi.org/10.1080/01431161.2012.700131

PLEASE SCROLL DOWN FOR ARTICLE

Full terms and conditions of use: http://www.tandfonline.com/page/terms-and-conditions

This article may be used for research, teaching, and private study purposes. Any substantial or systematic reproduction, redistribution, reselling, loan, sub-licensing, systematic supply, or distribution in any form to anyone is expressly forbidden.

The publisher does not give any warranty express or implied or make any representation that the contents will be complete or accurate or up to date. The accuracy of any instructions, formulae, and drug doses should be independently verified with primary sources. The publisher shall not be liable for any loss, actions, claims, proceedings, demand, or costs or damages whatsoever or howsoever caused arising directly or indirectly in connection with or arising out of the use of this material.

International Journal of Remote Sensing
Vol. 33, No. 22, 20 November 2012, 7273–7290

Taylor & Francis
Taylor & Francis Group

Spectral pathways for effective delineation of high-grade bauxites: a case study from the Savitri River Basin, Maharashtra, India, using EO-1 Hyperion data

K. N. KUSUMA, D. RAMAKRISHNAN* and H. S. PANDALAI
Department of Earth Sciences, Indian Institute of Technology, Mumbai 400076, India

(*Received 15 July 2010; in final form 26 April 2012*)

Bauxite, the only source of aluminium, is an aggregate of minerals, most of which are oxides and hydroxides of aluminium and iron such as gibbsite, bohemite, goethite and haematite. Bauxite is used in the chemical and refractory industries and its quality is controlled by the presence of impurities such as iron and silica. Bauxite commonly occurs together with iron-rich laterites as alteration products of parental igneous and metamorphic rocks. Aluminium-rich bauxites grade towards highly ferruginous laterites with a transitional Al-rich laterites or ferruginous bauxite, herein described as Al-laterites. In the Savitri River Basin, bauxite contains 58–75% gibbsite, 6–11% goethite and 19–26% haematite, whereas the mineralogy of Al-laterites and Fe-laterites are dominated by haematite (29–68%) and goethite (6–25%) with subordinate amounts of gibbsite. Conventional techniques to demarcate the high-grade pockets of bauxites rich in gibbsite are tedious, time consuming and involve detailed field sampling and geochemical analyses. Our work illustrates how spectral properties of these three litho-units can be effectively utilized in mapping of high-grade bauxites occurring over wide areas using hyperspectral remote sensing (HRS). The methodology adopted herein involves generation of noise-free field spectral database of target materials, linear unmixing of field spectra for constituent minerals, classification of preprocessed Hyperion images using field spectra and finally accuracy assessment for ore grade estimation. It is observed that bauxite mapping using Hyperion data and noise-free field spectra yielded results that correlate well with the chemistry and mineralogy of representative samples. By adopting the above procedure, we achieved classification accuracies of 100%, 71% and 89% for bauxite, Al-laterite and Fe-laterite classes, respectively.

Downloaded by [IIT Indian Institute of Technology - Mumbai] at 07:24 11 July 2012

1. Introduction

The study of the characteristic absorption features of minerals and their mixtures using discrete, broad channels of multispectral imagery, such as Landsat, Système Pour l'Observation de la Terre (SPOT) and Indian Remote Sensing (IRS) images, has serious limitations because of the large bandwidth of their channels, which makes them insensitive to wavelength-specific absorption features of minerals. Hyperspectral remote sensing (HRS), which uses the reflectance (or emissivity) spectra of an object in narrow, contiguous spectral bands, has overcome limitations of multispectral remote sensing for identifying minerals and rocks accurately (Goetz 2009). The identification

*Corresponding author. Email: ramakrish@iitb.ac.in

International Journal of Remote Sensing
ISSN 0143-1161 print/ISSN 1366-5901 online © 2012 Taylor & Francis
http://www.tandfonline.com
http://dx.doi.org/10.1080/01431161.2012.700131

Downloaded by [IIT Indian Institute of Technology - Mumbai] at 07:24 11 July 2012

of mineral and mineral aggregates (e.g. rocks and soils) using HRS data is based on the concept that each mineral has its characteristic spectral absorption feature shapes that depend on the structure and chemistry of crystal lattices of individual minerals, and the nature of their physical surfaces (Burns 1970, Hunt and Salisbuary 1970, Hunt *et al*. 1971, 1973, Goetz *et al*. 1985, Rossman 1988, Goetz 2009). Laboratory, field, airborne and spaceborne measurements of spectral signatures have proved to be useful in various fields of applications related to geology, such as lithologic mapping (Clark *et al*. 1992, Clark and Swayze 1995, Van der Meer *et al*. 1997, Rowan *et al*. 2004), mineral exploration (Kruse *et al*. 1993, Bierwirth *et al*. 2002, Cudahy 2004, Swayze *et al*. 2004) and hydrothermal alteration mineral mapping (Barley 1984, Crowley and Zimbelman 1997, Bierwirth *et al*. 2002, Kruse 2002, Kruse *et al*. 2003, 2006, Cudahy 2004, Kennedy-Bowdoin *et al*. 2004). HRS has also been used effectively to identify secondary mineral components constituting extensive areas of regolith (Das 1996, Carvalho *et al*. 1999, Papp and Cudahy 2002, Craig *et al*. 2006, Deller 2006). Our study is directed towards deciphering the boundaries of bauxite and aluminous (or Al-) laterites over ferrugenous (or Fe-) laterites.

Bauxite, an end product of residual weathering, is rich in aluminium hydroxides with low concentrations of iron, silica, alkalis and titanium. Besides being an ore of aluminium, bauxite is also used in the abrasives, chemical and refractory industries. The economic value of bauxite depends on the content of Al_2O_3 and other associated impurities such as Fe_2O_3, SiO_2 and TiO_2. Because of intimate mixing between the major oxide (and hydroxide) phases, it is nearly impossible to differentiate pure forms from impure forms, which would otherwise necessitate extensive field sampling and geochemical analyses to detect the more valuable grades of ore.

In this study, we demonstrate a method for discriminating and mapping the closely related bauxite, Al-laterite and Fe-laterite bodies within the Savitri River Basin area, Maharashtra, India, using visible through infrared field spectroscopy and HRS data. Our procedures involve (i) identification of mineral species and their abundances in field spectra by spectrally unmixing them using the United States Geological Survey (USGS) Mineral Spectral Library (Clark *et al*. 2007); (ii) discrimination of bauxites from Al-laterites and Fe-laterites based on their component mineral abundances; (iii) spatial mapping of high aluminous bauxites by matching field spectra with satellite (Hyperion) image spectra; and (iv) validation of the procedure for accuracy based on ground truth.

2. Study area

The Savitri River Basin area (figure 1) is bounded by the Western Ghat Escarpment (WGE), a steep geomorphic feature that rises about 1200 m above the Konkan Coastal Plain to its east and the Arabian Sea to its west. The Konkan Plain is a narrow strip of land about 65 km wide that lies between the western coastline of India and the WGE. This plain is divided into a coast-parallel strip extending landward about 42 km from the coast, called the Outer Konkan Plain (OKP) and another strip, called the Inner Konkan Plain (IKP), which extends from the eastern edge of the OKP up to the foothills of the coast-parallel WGE (Gunnell 2001, Kusuma 2010). The OKP is made up of a series of low plateaus, which generally increase in height from their western coastal side to their inland edges, where it occasionally reaches heights of 400 m. These plateaus are capped by laterites and are cut up by narrow gorges of short rivers that flow north–south to meet the Savitri River, which cuts a broad east–west valley amidst these laterite-capped plateaus.

Downloaded by [IIT Indian Institute of Technology - Mumbai] at 07:24 11 July 2012

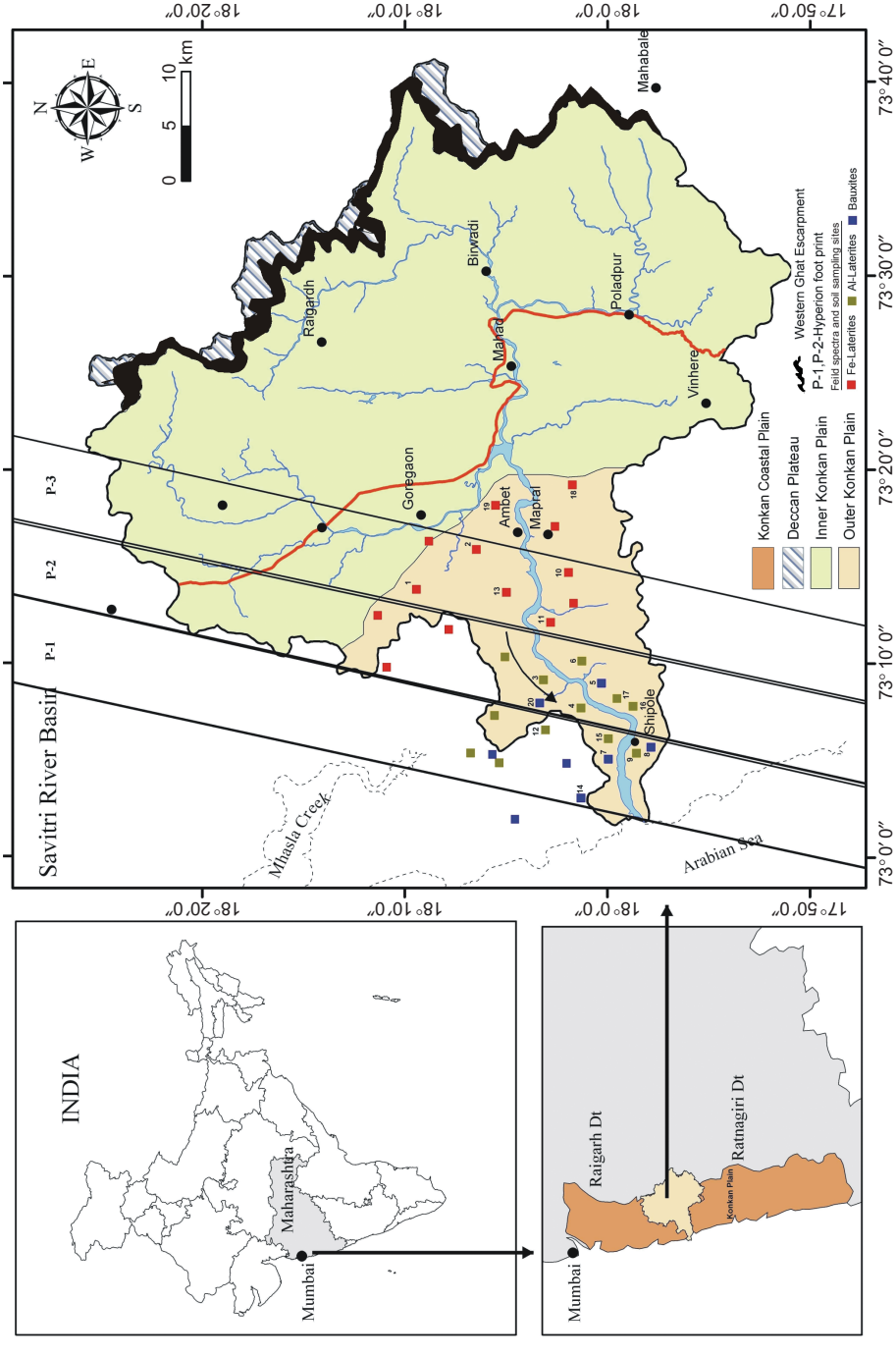

Figure 1. Location map of the Savitri River Basin indicating geomorphic divisions, sampling locations and Hyperion swaths.

The typical weathering profile in the field shows progressive transition from duricrust (laterite/ bauxite) in the top to unaltered basalt in the bottom through a mottled zone with saprolite in between (Walther 1915). In the western parts of the OKP, adjoining the coast, mineable reserves of 'pocket-type' bauxite deposits occur along with Al-laterites and Fe-laterites. The bauxite and Al-laterite deposits are exposed ubiquitously on the plateau top with or without a thin veneer of laterite gravels.

In the study area, the economic bauxite deposit is confined to a narrow strip as caps over weathering profiles developed on the Deccan basalt adjoining the coast. High-grade, commercially viable deposits in this area are discontinuous and patchy. Many of the transitional forms of ore, ranging between laterite and bauxite, can be observed with only a thin mantle of top soil/laterite gravel covering them. The surface expression of the deposits is dependent on the size and shape of the bauxite ore body and their enclosing litho-units. In general, the typical bauxite profiles consist of an upper, strongly indurated, dissected aluminium and/or iron-rich layer (duricrust) and a poorly preserved saprolite horizon having a gradational contact with the parent bedrock. In some areas, the weathering profiles are completely dissected and blocks of bauxite/laterites are strewn immediately atop the parent rocks. A typical bauxite profile (2.5–15 m thick) of the study area has the sequence of (i) duricrust, (ii) mottled horizon, (iii) pallid zone and (iv) basalt rock from top to bottom. The duricrust is typically coarse-grained with fragments of size ranging from 2 to 6 cm.

The landform features of the study area are mostly attributable to the pre-Neogene period, with modifications during the Neogene and Quaternary periods. Prior to these modifications, most of the study area was capped by a deeply weathered laterite crust. Changes in the local base level due to sea-level changes and tectonic activity resulted in the erosion of the weathered mantle in areas of high erosion potential (IKP and WGE regions). Areas of low erosion potential, such as OKP, retained their original weathering profiles. *In situ* regolith, occupying the tops of the present-day plateau, mesas and buttes, can be attributed to topographic relief inversion (Kusuma 2010).

3. Methodology

The methodology followed in this study involves (1) generation of a representative field spectral database for duricrusts and regoliths within our study area; (2) preprocessing of field spectra for noise reduction purposes; (3) deconvolution of field spectra; (4) Hyperion image analyses; and (5) mineralogical and geochemical analyses of field samples for grade estimation.

Biconical reflectances of Fe-laterites, bauxites and Al-laterites were measured at 50 field locations in the study area using an Analytical Spectral Devices (ASD) Fieldspec3 (Boulder, CO, USA) portable field spectroradiometer having a field of view (FOV) of 25°. The instrument was calibrated under solar illumination with the aid of a Spectralon panel (Labsphere, North Sutton, NH, USA). Field spectra were collected by keeping the sensor at 1 m above ground level with the Sun at its zenith and the sensor at about 10° from zenith. At each location, four consecutive spectral measurements were made with the accumulation of 20 co-adds. GPS coordinates were also obtained at the time of spectral measurements.

Notably, the field spectra (figure 2) contain wavelength-specific and non-specific coherent noises caused by atmospheric water vapour, gases, scattering and signal-to-noise ratio (SNR) limitations of the instrument (Schmidt and Skidmore 2004, Ramsey *et al*. 2005). Noise can obscure the characteristic shapes of fundamental,

Downloaded by [IIT Indian Institute of Technology - Mumbai] at 07:24 11 July 2012

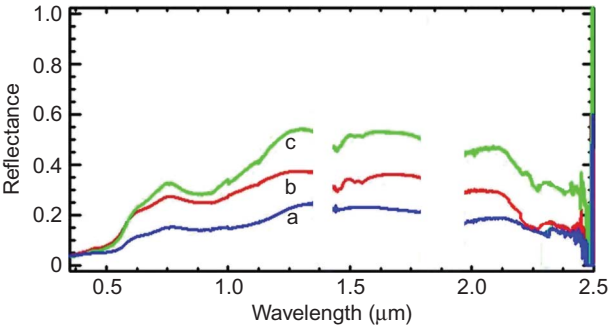

Figure 2. Field spectra of Fe-laterite (a), bauxite (b) and Al-laterite (c). Noises in water vapour absorption bands have been removed for clarity. Noise suppression (Kusuma *et al*. 2010) has been used subsequently to enhance the spectral quality, prior to their use in spectral classification of the Hyperion imagery.

Downloaded by [IIT Indian Institute of Technology - Mumbai] at 07:24 11 July 2012

overtone and combination absorption features of minerals and reduce the efficacy of spectral matching and mineral abundance estimates. From the field spectra, we eliminated the noise related to water vapour absorption at 1.4 and 1.9 μm. Subsequently, preprocessing of the field spectra was done with the aid of lab spectra before they were used for spectral mineral mapping and abundance estimation (Schaepman and Dangel 2000, Liu *et al*. 2006). In our study, we observed that the spectral absorption features correspond to the Fe–OH, Al–OH, Mg–OH and carbonate contents of duricrust and regolith minerals. These absorption features span the wavelength region between 2000 and 2500 nm and are mostly affected by spectrally coherent noise.

Preprocessing of field spectra representing Fe-laterite, Al-laterite and bauxite was carried out using the noise-to-signal index threshold procedure (Kusuma *et al*. 2010). These noise-corrected spectra were subsequently deconvolved to their mineralogical constituents (i.e. endmembers) and their fractional abundances using the USGS Spectral Library spectra (Clark *et al*. 2007) and by modelling linear mixtures of the major duricrust/regolith minerals in varying proportions. Fe-laterite, Al-laterite and bauxite can be considered as intimate mixtures (Clark 1999) that require a non-linear mixture model (Hapke 1981) for precise estimation of mineral abundances. However, considering the photometric roughness-related uncertainties due to the rugged topography (Hapke 1984, Domingue and Vilas 2007), we use the computationally simpler and reasonably satisfactory linear mixture model (LMM) to estimate the aerial fractional abundances of minerals. While deconvolving the Hyperion image spectra in non-vegetated areas, LMM was done using USGS Spectral Library spectra (Clark *et al*. 2007) of goethite, haematite and gibbsite, based on coarse fraction (>250 μ) measurements of these minerals. In sparsely vegetated areas, spectral signatures of vegetation were also included as one of the LMM endmembers.

Fifteen samples representing bauxite, Al-laterite and Fe-laterite were analysed for mineralogy and geochemistry. Mineralogical analyses were carried out on powder samples using a Rigaku (Shibuya-Ku, Tokyo, Japan) D/MaxIC Cu α X-ray diffractometer (XRD) with scanning angles (2θ) between 4° and 60°. Semi-quantitative estimates of mineralogy from XRD data were made following the procedures of Goehner (1982). For geochemistry, an X-ray fluorescence (Philips model PW2404, Almelo, The Netherlands) technique was used and the instrument was calibrated using the USGS standards Sco-1, SGR-1 and Sdo-1 (Govindaraju 1994).

Downloaded by [IIT Indian Institute of Technology - Mumbai] at 07:24 11 July 2012

Hyperion scenes (Level L1R product) covering part of the study area were processed using Environment for Visualizing Images (ENVI 4.5) software. The Hyperion radiance data were preprocessed for atmospheric effects and transformed to calibrated reflectance using the Fast Line-of-sight Atmospheric Analysis of Spectral Hypercubes (FLAASH) algorithm (Matthew *et al*. 2000). Atmospheric correction also included compensation for cross-track spectral shift and adjacency effects. Akin to field spectra, noisy Hyperion bands at 1.4 and 1.9 μm representing the atmospheric water vapour absorption region were also removed. Subsequently, spectrally coherent noise in the Hyperion image cube was smoothed using the EFFORT polishing (Boardman 1998) algorithm.

The incoherent noise component of the satellite data was evaluated by performing the minimum noise fraction (MNF) transformation. MNF transformation was carried out on a spectrally calibrated and smoothed reflectance image cube comprising 196 effective bands. The eigenvector plot and the MNF-transformed bands for each input image were examined. After critical evaluation, 30 MNF bands with eigenvalues more than 1.1 were selected for inverse MNF transformation. The resultant incoherent noise-corrected image cube was classified using three different spectral matching and classification techniques, namely spectral angle mapper (SAM – Kruse *et al*. 1993), spectral feature fitting (SSF – Clark *et al*. 1990) and binary encoding (BE – Mazer *et al*. 1988). We scaled the outputs of SAM (inverse of spectral angle similarity (in radians)), SSF (continuum-removed fits) and BE (average correlation fits) into a measure ranging between 0% and 100% and then weighted each by 33% (i.e. equal weighting) to yield an average-weighted spectral similarity score (AWSS). Although Crosta *et al*. (1998) suggested that SFF is better for classifying the iron-bearing alteration minerals, in our earlier work (Kusuma *et al*. 2010) we observed that SAM yields excellent classification results after spectrally coherent noises were removed from the field spectra of bauxite, Al-laterite and Fe-laterite. Hence, most of our interpretations in this study are based on either AWSS or SAM. The SAM classification was carried out with several spectral angle thresholds ranging from 0.1 to 0.4 for all of the three end-members. Each time, the classified output was compared with field data for accuracy and spectral angle optimization. When satisfactory threshold values were achieved, the classified images were geocorrected and mosaicked using Survey of India topographic maps re-projected using Universal Transverse Mercator (UTM) and World Geodetic Datum (WGS-84) projection parameters. The geometric correction is fairly accurate (with a root mean square error varying from 0.01 to 0.04) and comparable with field GPS measurements.

In particular, SAM is a classification method that calculates the similarity between two spectra. Spectral similarity between the two spectra is measured by the angle between two vectors representing the spectra in n-dimensional space with dimensionality equal to the number of bands (n_b) (Kruse *et al*. 1993, Van der Meer *et al*. 1997) as shown in the following equation:

$$\alpha = \cos^{-1}\left[\frac{\sum_i^{n_b} t_i r_i}{\left(\sum_{i=1}^{n_b} t_i^2\right)^{1/2}\left(\sum_{i=1}^{n_b} r_i^2\right)^{1/2}}\right], \tag{1}$$

where α is the spectral angle, t_i is the pixel spectrum, r_i is the reference spectrum and n_b is the number of bands.

The result of SAM analysis for each pixel is an angular similarity measured in radians ranging from zero to $\pi/2$, which gives a qualitative estimate of the presence of

absorption features that can be related to mineralogy (e.g. Van der Meer and Bakker 1997). For example, small angles between the two spectra indicate high similarity. However, SAM being a cumulative measure of similarity between two feature vectors, the presence of high frequency noise in reference and pixel spectra is expected to reduce the similarity measure. The accuracy of mapping was estimated in this study by (i) comparing spectral similarity between field spectra and pixel spectra and (ii) estimating the user and producer accuracies.

4. Results

4.1 *Mineralogy, chemistry, field and laboratory spectroscopy*

It is evident from semi-quantitative analysis of X-ray diffraction data (table 1) that the mineralogy of bauxite is dominated by gibbsite (58–75%) over other minerals such as haematite (19–26%) and goethite (6–11%). The Al-laterites contain gibbsite (32–42%), haematite (29–58%) and goethite (6–25%), while the Fe-laterites are composed mostly of haematite (55–68%), goethite (6–16%) and gibbsite (11–28%). In addition to these minerals, small percentages of minerals such as kaolinite, anatase, quartz and bohemite are also observed in many cases (figure 3). The pallid and mottled horizons (saprolite) consist of kaolinite, goethite, montmorillonite, altered plagioclase feldspar, augite, anatase and occasional quartz. Pellets of finely powdered samples representing the duricrusts (bauxite, Al-laterite and Fe-laterite) were also prepared for the study of bulk chemistry using X-ray flourometry. It is apparent from the results (table 1) that the bauxite is dominated by alumina (Al_2O_3 = 47–55%) with subordinate amounts of iron oxide (9.7–15.2%) and silica (3.3–4.8%). In the case of Al-laterites, the alumina content ranges from 26.4% to 39.2% with an almost equal amount of iron oxide (34.5–48.7%). Unlike the bauxites and Al-laterites, the Fe-laterite contains very high percentages of ferric iron oxide (48.6–56.0%).

The noise-free field spectra of targets of interest were analysed and interpreted in terms of mineralogical abundances by correlating continuum-removed field spectra with USGS Spectral Library of minerals. The spectra of bauxites exhibit strong Al–OH vibration features at wavelengths 2.26, 1.54 and 2.35 μm and weak features at 0.48 and 0.99 μm. Spectral Library mineral endmembers displaying the same absorption features include gibbsite, kaolinite and haematite. In addition to the absorption features at 2.26 and 1.54 μm, the Al-laterites have strong absorption features at 0.48, 0.60 and 0.94 μm regions. These absorption features can be attributed to the 'charge transfer' and 'crystal field' effects (Van Vleck 1932, Burns 1970) of iron-bearing minerals such as haematite, goethite and the Al–OH vibration absorption of gibbsite. The Fe-laterites have strong absorption features at 0.55 and 0.88 μm regions and weak features at 0.49, 2.20 and 2.40 μm regions corresponding to contributions from haematite, goethite and gibbsite. High SAM and SFF match scores of haematite (0.85 and 0.93) and gibbsite (0.87 and 0.79) with the field spectra also confirm the dominance of these two minerals in the field spectra of Fe-laterites, Al-laterites and bauxite.

Based on the LMM deconvolution results, it is evident from table 2 that the bauxite is predominantly composed of gibbsite (45–60%), haematite (35–45%) and goethite (5–10%). The mineralogy of Al-laterite varies from 20% to 40% of gibbsite, 50% to 70% of haematite and 5% to 10% of goethite. Similarly, the mineralogical composition of Fe-laterites suggests 70–75% haematite, 5–10% goethite and subordinate percentage of gibbsite (15–25%). Based on the highest AWSS (table 2), we arrived at

Downloaded by [IIT Indian Institute of Technology - Mumbai] at 07:24 11 July 2012

Downloaded by [IIT Indian Institute of Technology - Mumbai] at 07:24 11 July 2012

Table 1. Major oxide geochemistry and mineralogy of the duricrusts.

Sample ID	Type of duricrust	Geochemistry (wt. %)								Mineralogy (%)
		SiO_2	Al_2O_3	Fe_2O_3	CaO	MgO	K_2O	TiO_2	LOI	
1	Fe-laterite	11.9	17.4	48.6	0.7	0.6	0.4	3.67	17.3	Haematite (58.4), gibbsite (11.5), bohemite (10), goethite (16), anatase (4.1)
2	Fe-laterite	5.7	16.6	56.0	0.7	0.5	0.1	3.4	17.8	Haematite (58), gibbsite (29), goethite (9), bohemite (4)
3	Al-laterite	3.3	28.7	48.7	0.8	0.5	0.2	4.3	19.0	Gibbsite (37), haematite (44), anatase (9), goethite (10)
4	Al-laterite	3.8	39.2	34.5	0.7	0.5	0.2	3.8	20.3	Gibbsite (32), haematite (58), goethite (6), kaolinite (4)
5	Bauxite	4.8	47.2	15.2	0.2	0.1	0.1	2.7	29.4	Gibbsite (75), haematite (19), goethite (6)
6	Fe-laterite	7.3	20.4	52.8	0.7	0.6	0.4	2.6	18.6	Haematite (62), gibbsite (26), goethite (6), anatase (6)
7	Bauxite	3.3	54.9	9.7	0.7	0.4	0.2	4.3	26.7	Gibbsite (58), haematite (26), goethite (11), anatase (5)
8	Bauxite	3.9	49.7	14.3	0.3	0.1	0.1	3.1	27.8	Gibbsite (67), haematite (21), goethite (6), anatase (6)
9	Al-laterite	7.3	26.4	46.8	0.7	0.6	0.4	2.6	18.6	Gibbsite (42), haematite (29), goethite (25), anatase (4)
10	Fe-laterite	8.4	22.8	48.8	0.8	0.6	0.5	4.1	16.9	Haematite (68.4), gibbsite (13.7), bohemite (9.5), goethite (8.6)
11	Fe-laterite	6.3	22.9	50.3	0.8	0.6	0.4	3.6	19.8	Haematite (55), gibbsite (28), goethite (9), kaolinite (5), anatase (3)
12*	Al-laterite				NE					Gibbsite, haematite,
13*	Fe-laterite				NE					Haematite, gibbsite, goethite,
14*	Bauxite	3.6	54.6	14.0	0.6	0.1	0.1	3.7	23.3	Gibbsite, haematite, goethite, kaolinite
15*	Al-laterite				NE					Haematite, gibbsite, kaolinite

Notes: NE, not estimated.
*Mineralogy based on Raman laser spectroscopy.

Downloaded by [IIT Indian Institute of Technology - Mumbai] at 07:24 11 July 2012

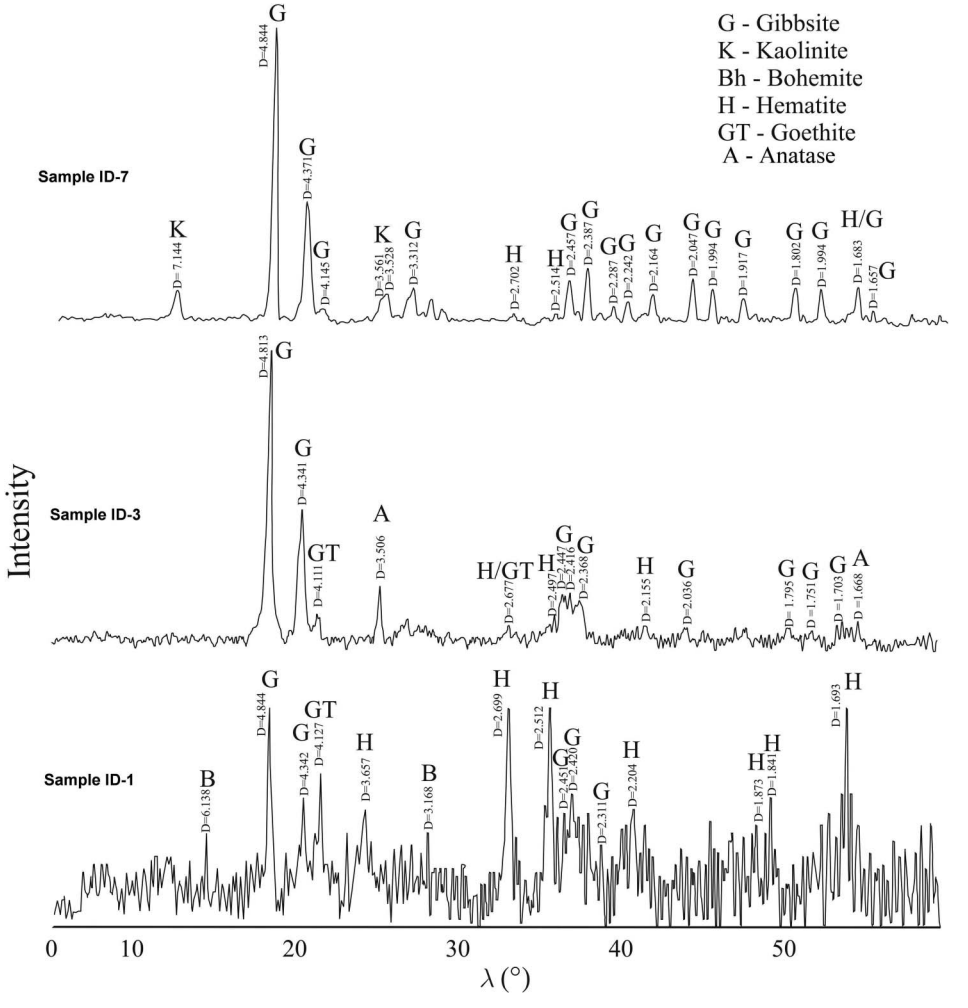

Figure 3. Representative X-ray diffractogram depicting the mineralogy of Fe-laterite (Sample ID-1), Al-laterite (Sample ID-3) and bauxite (Sample ID-7).

spectral mixtures representing bauxite (35% HT, 5% GT, 60% GB), Al-laterite (55% HT, 5% GT, 40% GB) and Fe-laterite (70% HT, 10% GT, 20% GB) (HT, haematite; GT, goethite; GB, gibbsite).

4.2 *Mapping high-grade bauxite exposures using Hyperion data*

The Hyperion image cube was classified using noisy and noise-free field spectra (figures 4(*a*) and (*b*)) with spectral angle thresholds of 0.30, 0.20 and 0.10 radians for bauxite, Al-laterite and Fe-laterite classes, respectively. These optimized spectral angles (estimated by iterative comparison between classification results and field data) gave the best possible classification accuracy.

Since the duricrusts are associated with plateau/mesa/butte tops, it is necessary to discriminate economically viable *in situ* bauxites from the non-economic, downslope-transported sediments rich in iron oxides and alumina. For this purpose,

Table 2. Linear mixtures of library spectra and spectral similarity scores for Fe-laterite, Al-laterite and bauxite samples.

Nature of deposit	Location no.	Mineralogical composition of the best match	SAM	SFF	BE	AWSS#
Fe-laterite	1	75% HT, 5% GT, 20% GB	69.9	96	88.2	84.8
	2	75% HT, 10% GT, 15% GB	76.6	99	77.9	84.8
	6	70% HT, 5% GT, 25% GB	82.5	91.2	88.6	87.8
	10	**70% HT, 10% GT, 20% GB**	**83.8**	**85**	**97.2**	**88.9**
Al-laterite	3	70% HT, 10% GT, 20% GB	86.3	85.6	86.8	85.9
	4	**55% HT, 5% GT, 40% GB**	**86.6**	**99.8**	**77.9**	**88.1**
	9	50% HT, 10% GT, 40% GB	88.4	79.2	87.5	81.9
	12	60% HT, 10% GT, 30% GB	77.6	71.8	77	75.8
Bauxite	5	**35%HT, 5%GT, 60%GB**	**84.9**	**94.9**	**88.9**	**89.9**
	7	45% HT, 10% GT, 45% GB	89.3	88.6	88.6	89.9
	8	45% HT, 5% GT, 50% GB	84.9	93.3	88.9	89.9
	14	45% HT, 10% GT, 45% GB	81.9	86.7	88.6	85.9

Notes: HT, haematite; GT, goethite; GB, gibbsite. AWSS# is the scaled outputs of SAM, SSF and BE into a measure ranging between 0% and 100% and then cumulated with equal weight (33%). Bold values indicate deconvloved mineral abundance of spectra used to classify the Hyperion image.

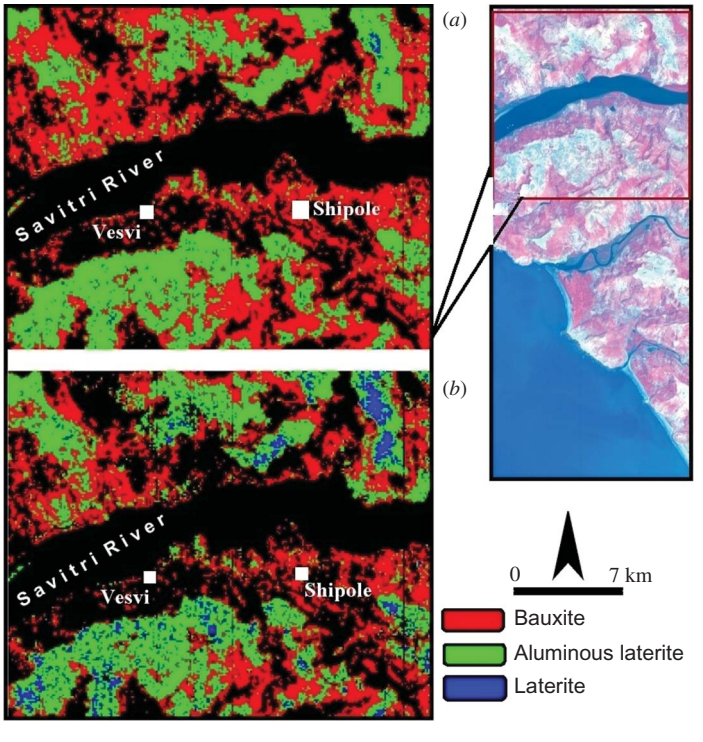

Figure 4. SAM classified maps for Fe-laterite, Al-laterite and bauxite generated using noisy field spectra (*a*) and noise-corrected field spectra (*b*).

Downloaded by [IIT Indian Institute of Technology - Mumbai] at 07:24 11 July 2012

a digital elevation model (DEM) of the study area was used to discriminate the *in situ* bauxite deposits from high aluminous sediments accumulated at lower topographic levels (<50 m AMSL). This map (figure 5) showing the distribution of *in situ* Fe-laterite, Al-laterite and bauxite was then evaluated for their classification accuracy by using two different procedures. In the first method, image and field spectra corresponding to bauxite, Al-laterite and Fe-laterite (figure 6) collected at 20 specific field locations were compared for spectral similarity (table 3). In the second technique, the classified output was compared with ground-truth information in the form of a confusion matrix (Congalton 1991). This was prepared by comparing the location and class of ground spots with the corresponding location and class in the classified

Downloaded by [IIT Indian Institute of Technology - Mumbai] at 07:24 11 July 2012

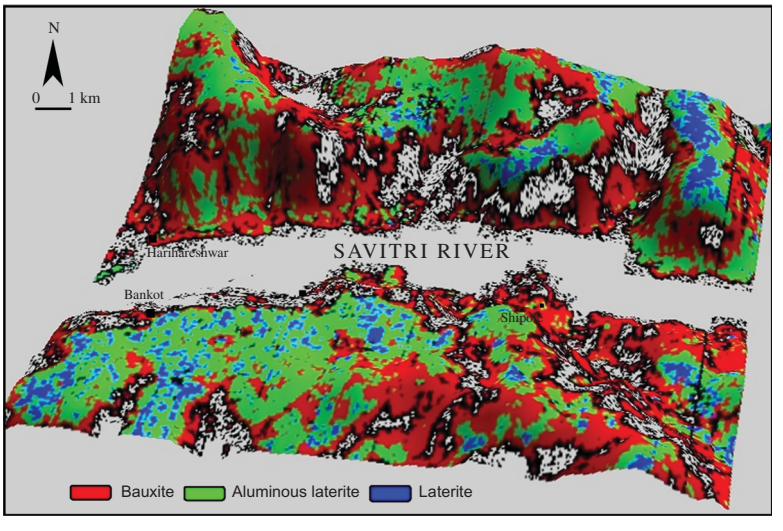

Figure 5. Overlay of classified map on DEM to discriminate the *in situ* and transported duricrusts.

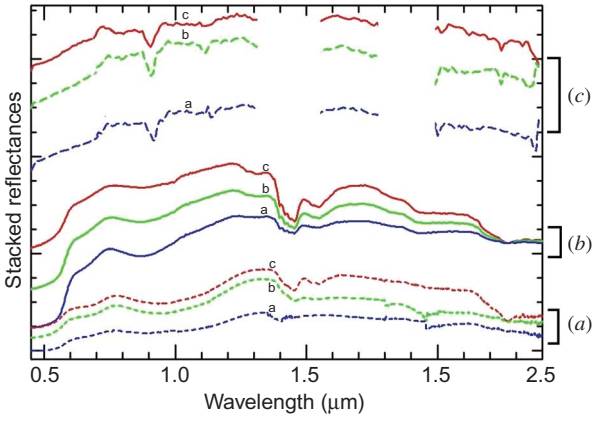

Figure 6. Stacked reflectance spectra of Fe-laterite (a), Al-laterite (b) and bauxite (c) representing noise-corrected field spectra (*a*), LMM mineral mixtures (*b*) and Hyperion pixel spectra (*c*).

Table 3. Spectral similarity measures (A) between field spectra and Hyperion pixel spectra and (B) between field spectra and USGS mineral mixtures.

	Noisy field spectra				Noise-corrected field spectra			
	SAM (%)	SFF (%)	BE (%)	AWSS# (%)	SAM (%)	SFF (%)	BE (%)	AWSS# (%)
(A) Matching score for Hyperion pixel spectra*								
Bauxite	33	61	66	52	71	66	94	76
Al-laterite	38	63	69	59	68	59	84	70
Fe-laterite	03	72	69	47	63	61	82	70
(B) Matching score for USGS mineral mixtures*								
Bauxite (35% HT, 5% GT, 60% GB)	68	93	79	80	85	95	89	90
Al-laterite (55% HT, 5% GT, 40% GB)	53	93	81	75	87	99	78	88
Fe-laterite (35% HT, 5% GT, 60% GB)	56	90	81	75	84	85	97	89

Note: *Median values of 20 sample points.

images (table 4). To understand the effect of spectrally coherent noise in reference spectra and its impact on classification accuracy, image cubes were classified using both noisy and noise-corrected reference spectra, and their classification accuracies were then compared (tables 3 and 4). It is evident from tables 3 and 4 that when noise was removed, the AWSS increased considerably for Fe-laterites (+23%), Al-laterites (+11%) and bauxites (+24%). A similar effect could also be noticed when AWSS was measured between the USGS mineral mixtures and reference spectra. Such an increase in the similarity score is mainly attributed to a significant increase in the SAM and BE scores. Based on the confusion matrix, it is obvious that the user's and producer's classification accuracies also significantly improved (table 4) after noise was removed from the reference spectra. Relating the duricrust distribution to slope and elevation (figure 6) helped us to augment further classification accuracies of Fe-laterite (89%), Al-laterite (71%) and bauxite (100%) classes.

5. Summary, discussion and conclusions

The Konkan region of India (figure 1) has proven reserves of about 10 million tons of various grades of bauxite deposits. These bauxite deposits are mostly confined to a narrow strip of coast parallel landform unit called OKP. This geomorphic unit has a gentle westward slope and is enveloped by lateritic regolith of varying compositions. Based on field studies, it is evident that the composition of the duricrust varies spatially from iron-rich facies (Fe-laterite) to aluminium-rich facies (bauxite). Considering the economic viability of aluminium resources, we were able to classify them into three categories: Fe-laterite, Al-laterite and bauxite, based on their total iron and aluminium contents. The percentages of alumina and iron oxide considered for qualifying a duricrust as bauxite are over 46% of Al_2O_3 and less than 18% of Fe_2O_3 respectively (Anand *et al*. 1991). Duricrusts with a relatively higher percentage of both Al_2O_3 (28–39%) and Fe_2O_3 (34–45%), but not amenable to the present ore processing technology, are

Downloaded by [IIT Indian Institute of Technology - Mumbai] at 07:24 11 July 2012

Table 4. Accuracy estimates for classification made using (A) noisy field spectra, (B) noise smoothened field spectra and (C) noise smoothened spectra and DEM.

		Fe-laterite	Al-laterite	Bauxite	Unclassified	Total samples	User's accuracy (%)
(A) Classification statistics using noisy spectra							
Class1	Fe-laterite	0	4	2	12	18	0.00
Class2	Al-laterite	4	6	0	4	14	42.86
Class3	Bauxite	0	0	4	2	6	66.67
Class4	Unclassified	0	0	2	2	4	
		4	10	8	20	42	
Producer's accuracy (%)		0.00	60.00	50.00			
Overall accuracy (%)	23.81						
(B) Classification statistics using noise-corrected spectra							
Class1	Fe-laterite	14	4	0	0	18	77.78
Class2	Al-laterite	4	8	0	2	14	57.14
Class3	Bauxite	0	0	6	0	6	100.00
Class4	Unclassified	0	0	4	0	4	
		18	12	10	2	42	
Producer's accuracy (%)		77.78	66.67	60.00			
Overall accuracy (%)	66.67						
(C) Classification statistics using noise-corrected spectra and topographic corrections							
Class1	Fe-laterite	16	2	0	0	18	88.89
Class2	Al-laterite	2	10	0	2	14	71.43
Class3	Bauxite	0	0	8	0	8	100.00
Class4	Unclassified	0	0	2	0	2	
		18	12	10	2	42	
Producer's accuracy (%)		88.89	83.33	80.00			
Overall accuracy (%)	80.95						

typically designated as Al-laterites. All other types of duricrusts with very high iron content ($Fe_2O_3 > 45\%$) are referred to as Fe-laterites. In the study area, we observed that the bauxite deposits often spatially grade into Al-laterites and Fe-laterites, which can result in the mining of inferior grade ores and production of rejected stock piles. The conventional approach for mapping high-grade bauxites involves detailed field mapping, sampling and extensive chemical and mineralogical analyses.

In this study, we took advantage of the advancements in field and satellite spectroscopic techniques (figure 7) for distinguishing higher grade bauxite ores from each other and other types of lateritic duricrust deposits. This was done using representative field spectra. Field spectra often contain spectrally coherent noise from various sources. In this study, noise-corrected reference spectra representing bauxites, Al-laterites and Fe-laterites were generated using the noise-to-signal index threshold technique (Kusuma *et al*. 2010).

Downloaded by [IIT Indian Institute of Technology - Mumbai] at 07:24 11 July 2012

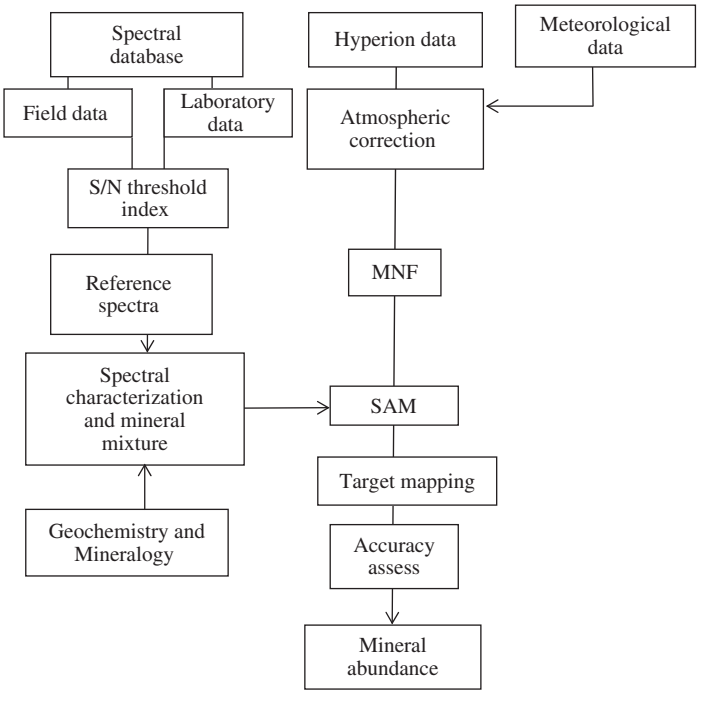

Figure 7. Workflow depicting the adopted procedures.

Considering the complexities of the intimate mixture modelling in terrains with high photometric roughness, such as Savitri Basin, LMM was carried out to estimate the aerial abundances of the three target groups. Linear unmixing of the field spectra with the aid of Spectral Library data revealed that the spectra of duricrusts are dominated by the minerals gibbsite and haematite, with lesser amounts of goethite. Based on weighted averages of rescaled spectral similarity outputs such as SAM, SFF and BE (collectively, AWSS), linear mixtures comprising 60% gibbsite, 35% haematite and 5% goethite were found to have the highest spectral match score (89.9%) for bauxite spectra. Similarly, Al-laterite spectra are best represented by linear mixtures of gibbsite (40%), haematite (55%) and goethite (5%). The Fe-laterite spectra correspond best to a mixture of 10% gibbsite, 70% haematite and 10% goethite. The laboratory data on geochemistry and mineralogy of all the three duricrusts commensurate well with the results deconvolved using field spectroscopy.

To understand the effect of spectral noise on classification, we used spectral similarity scores and user and producer accuracies as measures of classification efficacy. It is apparent from the results that noise correction significantly improved spectral classification between reference spectra and image spectra in all the three classes. The same results were obtained when noise-corrected spectra were matched with USGS mineral mixtures. It is interesting to observe from table 2 that the SFF technique seems to be more effective in classifying the laterites and bauxite than SAM and BE techniques. However, the efficacy of SAM and BE classification increased considerably when noise-free reference spectra were used (table 3, figure 5).

Although satellite multispectral imagery has been used to map bauxites, laterites and regoliths by various workers globally (Hickey 2005, Deller 2006, Sanjeevi 2008),

Downloaded by [IIT Indian Institute of Technology - Mumbai] at 07:24 11 July 2012

multispectral imagery lacks the spectral resolution (i.e. smaller number of bands and broader band passes) for estimating mineral abundances as compared to hyperspectral imagery such as EO-1 Hyperion.

The following conclusions emerge from this study.

1. The procedure adopted involving field spectroscopy and Hyperion data analysis is capable of distinguishing bauxite from other lateritic-duricrust types of lesser economic value.
2. When noise-free field spectra are used for classification, Fe-laterite was more clearly discriminated from Al-laterite, and the classification accuracy in all the three classes increased significantly.
3. When representative reference spectra are deconvolved to estimates of their mineral abundances, it is possible to classify images directly to those same mineral abundance classes. In this study, LMM produced reasonably good mineral abundance estimates for Fe-, Al-laterites and bauxitic duricrusts. Besides the limitations of LMM, we observed that mineral abundances estimated from spectroscopy match well with mineralogy estimated by XRD and geochemistry estimated by X-ray fluorescence procedures. Thus, spectroscopy can be used as a proxy for conventional exploration procedures for bauxites.
4. Combining classification outputs with slope and other topographic attributes derived from a DEM facilitated the identification of *in situ* bauxites from lower grade colluvial deposits on the lower slopes. This procedure further improves classification accuracy.

Downloaded by [IIT Indian Institute of Technology - Mumbai] at 07:24 11 July 2012

Acknowledgements

We are thankful to both anonymous reviewers for their constructive criticism. DR is obliged to one of the anonymous reviewers who took personal interest in this work. His critical comments and editing significantly helped in improving the quality of this article.

References

Anand, R.R., Gilkes, R.J. and Roach, G.I.D., 1991, Geochemical and mineralogical characteristics of bauxites, Darling Range, Western Australia. *Applied Geochemistry*, **6**, pp. 233–248.

Barley, M.E., 1984, Volcanism and hydrothermal alteration, Warrawoona Group, East Pilbara. In *Archaean and Proterozoic Basins of the Pilbara, Western Australia – Evolution and Mineralization Potential*, J.R. Muhling, D.I. Groves and T.S. Blake (Eds.), pp. 23–26 (Perth, WA: University of Western Australia).

Bierwirth, P., Huston, D. and Blewett, R., 2002, Hyperspectral mapping of mineral assemblages associated with gold mineralization in the Central Pilbara, Western Australia. *Economic Geology*, **97**, pp. 819–826.

Boardman, J.W., 1998, Post-ATREM polishing of AVIRIS apparent reflectance data using EFFORT: a lesson in accuracy versus precision. In *Summaries of the 7th JPL Airborne Earth Science Workshop*, 12–16 January 1998, Pasadena, CA (JPL Publication 97-21), vol. 1, p. 53.

Burns, R., 1970, *Mineralogical Applications of Crystal Field Theory*, 224 p. (Cambridge: Cambridge University Press).

Carvalho Jr., A.A.D., Der De Martins, S., De Mello Baptista, G.M., De Carvalho, A.P.F., Da Silva Madeira Netto, J. and Meneses, P.R., 1999, Mineralogical differentiation in weathering profiles of lateritic Ni using Aviris data. In *Summaries of*

8th JPL Airborne Earth Sciences Workshop, Pasadena, CA (JPL Publication 99-17), pp. 3–11.

Clark, R.N., 1999, Spectroscopy of rocks and minerals, principles of spectroscopy. In *Manual of Remote Sensing*, A. Rencz, (Ed.), 3rd ed., pp. 3–58 (New York: Wiley).

Clark, R.N., Gallagher, A.J. and Swayze, G.A., 1990, Material absorption band depth mapping of imaging spectrometer data using the complete band shape least-squares algorithm simultaneously fit to multiple spectral features from multiple materials. In *Proceedings of the 3rd Airborne Visible/Infrared Imaging Spectrometer (AVIRIS) Workshop*, Padasena, CA (JPL Publication 90-54), pp. 176–186.

Clark, R.N. and Swayze, G.A., 1995, Mapping minerals, amorphous materials, environmental materials, vegetation, water, ice and snow, and other materials: the USGS Tricorder Algorithm. In *5th Annual JPL Airborne Earth Science Workshop*, 23–26 January 1995, R.O. Green (Ed.), Padasena, CA (JPL Publication 95-1), pp. 39–40.

Clark, R.N., Swayze, G.A. and Gallagher, A., 1992, Mapping the mineralogy and lithology of Canyonlands, Utah with imaging spectrometer data and the multiple spectral feature mapping algorithm. In *Summaries of the 3rd Annual JPL Airborne Geoscience Workshop*, Padasena, CA (JPL Publication 92-14), pp. 11–13.

Clark, R.N., Swayze, G.A., Wise, R., Livo, K.E., Hoefen, T.M., Kokaly, R.F. and Sutley, S.J., 2007, USGS Digital Spectral Library splib06a, US Geological Survey, Data Series 231.

Congalton, R., 1991, A review of assessing the accuracy of classification of remotely sensed data. *Remote Sensing of Environment*, **37**, pp. 35–46.

Craig, S.E., Lohrenz, S.E., Lee, Z., Mahoney, L.M., Kirkpatrick, G.J., Schofield, M. and Steward, R.G., 2006, Use of hyperspectral remote sensing reflectance for detection and assessment of the harmful alga, Karenia brevis. *Applied Optics*, **45**, pp. 5414–5425.

Crosta, A.P., Sabine, C. and Taranik, J.V., 1998, Hydrothermal alteration mapping at Bodie, California, using AVIRIS hyperspectral data. *Remote Sensing of Environment*, **65**, pp. 309–319.

Crowley, J.K. and Zimbelman, D.R., 1997, Mapping hydrothermally altered rocks on Mount Rainier, Washington, with Airborne Visible/Infrared Imaging Spectrometer (AVIRIS) data. *Geology*, **25**, pp. 559–562.

Cudahy, T.J., 2004, Mapping alteration zonation associated with volcanic massive sulphide mineralisation using airborne hyperspectral data. In *CSIRO Explores: Copper – Zinc Massive Sulphide Deposits in Western Australia*, T.F. McConachy and B.A.I. McInnes (Eds.), vol. 2, pp. 117–124 (Perth, WA: CSIRO).

Das, I.C., 1996, Spectral signatures and spectral mixture modeling as a tool for targeting aluminous laterite and bauxite ore deposits, Koraput, India. GIS Development. Available online at: http://www.gisdevelopment.net/application/geology/mineral/geom0017pf.htm

Deller, A.M.E., 2006, Facies discrimination in laterites using Landsat Thematic Mapper, ASTER and ALI data – examples from Eritrea and Arabia. *International Journal of Remote Sensing*, **27**, pp. 2389–2409.

Domingue, D. and Vilas, F., 2007, Local topographic effects on photometry and reflectance spectra of planetary surfaces: an example based on lunar photometry. *Meteoritics and Planetary Science*, **42**, pp. 1801–1816.

Goehner, R.P., 1982, X-ray diffraction quantitative analysis using intensity ratios and external standards. *Advances in X-ray Analysis*, **25**, pp. 309–313.

Goetz, A.F.H., 2009, Three decades of hyperspectral remote sensing of the Earth: a personal view. *Remote Sensing of Environment*, **113**, pp. S5–S16.

Goetz, A.F.H., Vane, G., Solomon, J.E. and Rock, B.N., 1985, Imaging spectrometry for earth remote sensing. *Science*, **228**, pp. 1147–1153.

Govindaraju, K., 1994, Compilation of working values and descriptions for 383 Geostandards. *Geostandards Newsletter*, **18**, pp. 1–158.

Downloaded by [IIT Indian Institute of Technology - Mumbai] at 07:24 11 July 2012

Gunnell, Y., 2001, Dynamics and kinematics of rifting and uplift at the Western Continental margin of India: insights from geophysical and numerical models. *Geological Society of India*, **47**, pp. 475–496.

Hapke, B., 1981, Bidirectional reflectance spectroscopy: 1. theory. *Journal of Geophysical Research*, **86**, pp. 3039–3054.

Hapke, B., 1984, Bidirectional reflectance spectroscopy: 3. Correction for macroscopic roughness. *Icarus*, **59**, pp. 41–59.

Hickey, R.J., 2005, An investigation of the multispectral response patterns of west Australian bauxite deposits. *Journal of Spatial Science*, **50**, pp. 97–113.

Hunt, G.R. and Salisbury, J.W., 1970, Visible and near infrared spectra of minerals and rocks. I. Silicate minerals. *Modern Geology*, **1**, pp. 283–300.

Hunt, G.R., Salisbury, J.W. and Lenhoff, C.J., 1971, Visible and near infrared spectra of minerals and rocks. III. Oxides and hydroxides. *Modern Geology*, **2**, pp. 195–205.

Hunt, G.R., Salisbury, J.W. and Lenhoff, C.J., 1973, Visible and near infrared spectra of minerals and rocks. VI. Additional silicates. *Modern Geology*, **4**, pp. 85–106.

Kennedy-Bowdoin, T., Silver, E.A. and Pickles, W.L., 2004, Geothermal prospecting using hyperspectral imaging and field observation, Dixie meadows, Nevada. *Geothermal Resources Council Transactions*, **28**, pp. 19–22.

Kruse, F.A., 2002, Comparison of AVIRIS and Hyperion for Hyperspectral Mineral Mapping. In *Proceedings 11th JPL Airborne Geoscience Workshop*, 4–8 March 2002, Pasadena, CA (JPL Publication 03-4) (CD-ROM).

Kruse, F.A., Boardman, J.W. and Huntington, J.F., 2003, Comparison of Airborne Hyperspectral Data and EO-1 Hyperion for mineral mapping. *IEEE Transactions on Geoscience and Remote Sensing (TGARS)*, **41**, pp. 1388–1400.

Kruse, F.A., Lefkoff, A.B., Boardman, J.B., Heidebrecht, K.B., Shapiro, A.T., Barloon, P.J. and Goetz, A.F.H., 1993, The Spectral Image Processing System (SIPS) – interactive visualization and analysis of imaging spectrometer data. *Remote Sensing of the Environment*, **44**, pp. 145–163.

Kruse, F.A., Perry, S.L. and Caballero, A., 2006, District-level mineral survey using airborne hyperspectral data, Los Menucos, Argentina. *Annals of Geophysics (Annali di Geofisica)*, **49**, pp. 83–92.

Kusuma, K.N., 2010, Imaging spectroscopy of lateritic regolith of the Savitri river basin, Maharashtra, India with special reference to laterite landform evolution. Unpublished PhD thesis, Indian Institute of Technology Bombay, India.

Kusuma, K.N., Ramakrishnan, D., Pandalai, H.S. and Kailash, G., 2010, Noise-signal index threshold: a new noise reduction technique for generation of reference spectra and efficient hyperspectral image classification. *Geocarto International*, **25**, pp. 569–580.

Liu, D., Zhang, Y., Zhang, B., Song, K., Wang, Z., Duan, H. and Li, F., 2006, Effects of sensor noise in spectral measurements on chlorophyll-a retrieval in Nanhu Lake of Changchun, China. *Journal of Electromagnetic Waves and Applications*, **20**, pp. 547–557.

Matthew, M.W., Adler-Golden, S.M., Berk, A., Richtsmeier, S.C., Levine, R.Y., Bernstein, L.S., Acharya, P.K., Anderson, G.P., Felde, G.W., Hoke, M.P., Ratkowski, A., Burke, H.-H., Kaiser, R.D. and Miller, D.P., 2000, Status of atmospheric correction using a MODTRAN4-based algorithm. In *SPIE Proceedings, Algorithms for Multispectral, Hyperspectral, and Ultraspectral Imagery VI*, 24–26 April 2000, S.S. Shen and M.R. Descour (Eds.), Orlando, FL (Bellingham, WA: SPIE Publications), vol. 4049, pp. 199–207.

Mazer, A.S., Martin, M., Lee, M. and Solomon, J.E., 1988, Image processing software for imaging spectrometry data analysis. *Remote Sensing of Environment*, **24**, pp. 201–210.

Papp, E. and Cudahy, T., 2002, Hyperspectral remote sensing. In *Geophysical and Remote Sensing Methods for Regolith Exploration*, E. Papp (Ed.), pp. 13–21, Open File Report, 144 (Canberra, ACT: CRC LEME).

Downloaded by [IIT Indian Institute of Technology - Mumbai] at 07:24 11 July 2012

Ramsey III, E., Rangoonwala, A., Nelson, G., Ehrlich, R. and Martella, K., 2005, Generation and validation of characteristic spectra from EO1 Hyperion image data for detecting the occurrence of the invasive species, Chinese tallow. *International Journal of Remote Sensing*, **26**, pp. 1611–1636.

Rossman, G.R., 1988, Vibrational spectroscopy of hydrous components. In *Reviews in Mineralogy*, F.C. Hawthorne (Ed.), vol. 18, pp. 193–206 (Germantown, NY: Mineralogical Society of America).

Rowan, L.C., Simpson, C.J. and Mars., J.C., 2004, Hyperspectral analysis of the ultramafic complex and adjacent lithologies at Mordor, NT, Australia. *Remote Sensing of Environment*, **91**, pp. 419–431.

Sanjeevi, S., 2008, Targeting limestone and bauxite deposits in southern India by spectral unmixing of hyperspectral image data. *Photogrammetry, Remote Sensing and Spatial Information Sciences*, **37**, pp. 1189–1194.

Schaepman, M.E. and Dangel, S., 2000, Solid laboratory calibration of non-imaging spectro-radiometer. *Applied Optics*, **39**, pp. 3754–3764.

Schmidt, K.S. and Skidmore, A.K., 2004, Smoothing vegetation spectra with wavelets. *International Journal of Remote Sensing*, **25**, pp. 1167–1184.

Swayze, G.A., Higgins, C.T., Clinkenbeard, J.P., Kokaly, R.F., Clark, R.N., Meeker, G.P. and Sutley, S.J., 2004, *Preliminary Report on Using Imaging Spectroscopy to Map Ultramafic Rocks, Serpentinites, and Tremolite-Actinolite-Bearing Rocks in California*, US Geological Survey Open-File Report 2004–1304, 20 p.

Van der Meer, F. and Bakker, W., 1997, CCSM: cross correlogram spectral matching. *International Journal of Remote Sensing*, **18**, pp. 1197–1201.

Van der Meer, F., Vazquez, T.M. and Van Dijk, P.M., 1997, Spectral characterization of ophiolite lithologies in the Troodos Ophiolite complex of Cyprus and its potential in prospecting for massive sulphide deposits. *International Journal of Remote Sensing*, **18**, pp. 1245–1257.

Van Vleck, J., 1932, Theory of the variations in paramagnetic anisotropy among different salts of the iron group. *Physical Review*, **41**, pp. 208–215.

Walther, J., 1915, Laterite in West Australien. *Zeitchrift der Deutschen Geologischen Gesellschaft*, **67**, pp. 113–140.

Downloaded by [IIT Indian Institute of Technology - Mumbai] at 07:24 11 July 2012